HHS Public Access

Author manuscript

Bone. Author manuscript; available in PMC 2017 July 01.

Published in final edited form as:

Bone. 2016 July ; 88: 39–46. doi:10.1016/j.bone.2016.04.003.

Deterioration of Trabecular Plate-Rod and Cortical Microarchitecture and Reduced Bone Stiffness at Distal Radius and Tibia in Postmenopausal Women with Vertebral Fractures

Ji Wang[1], **Emily M. Stein**[2], **Bin Zhou**[1], **Kyle K. Nishiyama**[2], **Y. Eric Yu**[1], **Elizabeth Shane**[2], and **X. Edward Guo**[1]

Ji Wang: jw2857@columbia.edu; Emily M. Stein: es2029@cumc.columbia.edu; Bin Zhou: bz2159@columbia.edu; Kyle K. Nishiyama: kn2205@cumc.columbia.edu; Y. Eric Yu: yy2407@columbia.edu; Elizabeth Shane: es54@cumc.columbia.edu; X. Edward Guo: exg1@columbia.edu

[1]Bone Bioengineering Laboratory, Department of Biomedical Engineering, Columbia University, New York, New York, USA

[2]Department of Medicine, College of Physicians and Surgeons, Columbia University, New York, New York, USA

Abstract

Postmenopausal women with vertebral fractures have abnormal bone microarchitecture at the distal radius and tibia by HR-pQCT, independent of areal BMD. However, whether trabecular plate and rod microarchitecture is altered in women with vertebral fractures is unknown. This study aims to characterize the abnormalities of trabecular plate and rod microarchitecture, cortex, and bone stiffness in postmenopausal women with vertebral fractures. HR-pQCT images of distal radius and tibia were acquired from 45 women with vertebral fractures and 45 control subjects without fractures. Trabecular and cortical compartments were separated by an automatic segmentation algorithm and subjected to individual trabecula segmentation (ITS) analysis for measuring trabecular plate and rod morphology and cortical bone evaluation for measuring cortical thickness and porosity, respectively. Whole bone and trabecular bone stiffness were estimated by finite element analysis. Fracture and control subjects did not differ according to age, race, body mass index, osteoporosis risk factors, or medication use. Women with vertebral fractures had thinner cortices, and larger trabecular area compared to the control group. By ITS analysis, fracture subjects had fewer trabecular plates, less axially aligned trabeculae and less trabecular connectivity at both the radius and the tibia. Fewer trabecular rods were observed at the radius. Whole bone stiffness and trabecular bone stiffness were 18% and 22% lower in women with vertebral fractures at the radius, and 19% and 16% lower at the tibia, compared with controls. The estimated failure load of the radius and tibia were also reduced in the fracture subjects by 13% and 14%, respectively. In summary, postmenopausal women with vertebral fractures had both

---

The authors have nothing to disclose

Authors' roles: Study design: XEG, EMS, and ES. Data collection: EMS and KKN. Data analysis: JW and BZ. Data interpretation: all authors. Drafting manuscript: JW. Revising manuscript content and approving final version of manuscript: all authors.

trabecular and cortical microstructural deterioration at the peripheral skeleton, with a preferential loss of trabecular plates and cortical thinning. These microstructural deficits translated into lower whole bone and trabecular bone stiffness at the radius and tibia. Our results suggest that abnormalities in trabecular plate and rod microstructure may be important mechanisms of vertebral fracture in postmenopausal women.

Keywords

Bone microarchitecture; High-resolution peripheral quantitative computed tomography; Individual trabecula segmentation; Vertebral fracture; Trabecular plate and rod

Introduction

Osteoporosis is a major disease of aging, characterized by low bone mass and microarchitectural deterioration of trabecular and cortical bone that lead to increased bone fragility and susceptibility to fractures.[1] Vertebral fractures are the most common osteoporotic fractures, occurring in nearly 25% of postmenopausal women,[2,3] and are associated with substantial increase in the risk of both future vertebral and non-vertebral fractures.[4–6] Assessment of microarchitecture and mechanical properties of bone at the distal radius and tibia using high resolution peripheral quantitative computed tomography (HR-pQCT) has increased the understanding of the structural abnormalities underlying vertebral fractures.[7]

Vertebral fractures are the direct result of deterioration of vertebral microarchitecture with collapse of weakened vertebral bodies. Recent findings suggest that patients with vertebral fractures also have extensive deterioration of trabecular and cortical microarchitecture at peripheral skeletal sites. [8–11] At the distal radius and tibia, postmenopausal women with vertebral fractures have been shown to have fewer and more widely spaced trabeculae, and thinner cortices compared with women without fractures. HR-pQCT is a noninvasive, three-dimensional (3D) high-resolution imaging technique that measures volumetric bone mineral density (BMD) of distal radius and tibia, and can visualize fine details of trabecular and cortical microarchitecture at 82μm voxel size.[12–14] Several HR-pQCT studies have demonstrated differences in microarchitecture and stiffness between subjects with osteoporotic fractures and non-fractured controls. [7,15–18] Moreover, techniques based on HR-pQCT images have been developed that provide greater insights into skeletal microarchitecture and mechanical properties. HR-pQCT-based micro finite element analysis (μFEA) computationally predicts bone stiffness, which has been useful in distinguishing fracture status.[12,16,19] Automatic segmentation algorithms have been developed to distinguish the cortical and trabecular compartments of distal radius and tibia.[20] A newly developed cortical structure evaluation method measures porosity and thickness of the cortex, important determinants of whole bone strength.[21,22] Individual trabecula segmentation (ITS)-based morphological analysis directly measures individual trabeculae, and characterizes trabecular type (plate and rod), orientation, and connectivity of trabecular plate and rod network.[23–26] Because trabecular plates and rods of various orientations have different roles in determining mechanical properties of trabecular bone, ITS assessment of

trabecular microarchitecture adds a unique perspective to bone fragility.[27–32] Studies using ITS have shown postmenopausal women with a history of fragility fractures have significantly lower trabecular plate volume, number and connectivity, regardless of aBMD by DXA, suggesting that trabecular plate microarchitectural abnormalities may increase the risk for osteoporotic fractures, over and above that associated with low BMD by DXA.[8,32,33] However, no studies have focused exclusively on vertebral fracture patients.

The goal of this study was to characterize the alterations of trabecular and cortical microarchitecture, with a focus on plate and rod microarchitecture, and bone stiffness at the distal radius and distal tibia in postmenopausal women with vertebral fractures. We hypothesized that postmenopausal women with vertebral fractures have fewer trabecular plates, less trabecular connectivity, more porous and thinner cortices, and lower bone stiffness at distal tibia and distal radius compared with non-fractured controls.

Materials and Methods

Subjects

In this study, we included 45 vertebral fracture subjects and 45 control subjects who matched with the fracture subjects according to age and race, from a subset of subjects previously described by Stein and colleagues.[8,10,11] 20 vertebral fracture cases in this cohort were reported in Liu et al and Stein et al. [8,10] Postmenopausal women, over age 60 years or more than 10 years postmenopause, were recruited at Columbia University Medical Center (CUMC; New York, NY, USA) or Helen Hayes Hospital (HHH; West Haverstraw, NY, USA) by advertisement, self-referral, or physician referral. Subjects were eligible for inclusion as vertebral fracture cases if they had a history of a low-trauma vertebral fracture that occurred after menopause or were found to have vertebral fractures by spine X-ray. Low trauma was defined as equivalent to a fall from a standing height or less. Vertebral fractures were identified by spine X-rays according to the semiquantitative method of Genant et al.[34] Vertebrae were graded as normal, or with mild, moderate, or severe deformities, defined as reductions in anterior, middle, or posterior height of 20– 25%, 25–40%, and >40%, respectively. Control subjects had no history of low-trauma fractures at any site and no vertebral deformity on lateral radiograph, as dictated by pre-specified exclusion criteria. There were no BMD requirements for inclusion. Potential cases and controls were excluded if they had endocrinopathies (*e.g.,* untreated hyperthyroidism, Cushing's syndrome, prolactinoma), celiac or other gastrointestinal diseases, abnormal mineral metabolism (*e.g.,* clinical osteomalacia, primary hyperparathyroidism), malignancy except for skin cancer, and drug exposures that could affect bone metabolism (*e.g.,* glucocorticoids, anticonvulsants, anticoagulants, methotrexate, aromatase inhibitors, thiazolidinediones). Women using hormone replacement therapy or raloxifene were permitted to participate. Women who had ever used teriparatide, or who had taken bisphosphonates for more than 1 year were excluded. All subjects provided written informed consent and the Institutional Review Board of Columbia University Medical Center approved this study. At the study visit, past medical history, reproductive history, and medication use were assessed. A physical exam was performed including height and weight.

Areal BMD

Areal BMD (aBMD) was measured by DXA (QDR-4500; Hologic Inc., Walton, MA, at CUMC; Lunar Prodigy, GE, Madison, WI, at HHH) of lumbar spine L1-L4 (LS), total hip (TH), femoral neck (FN), 1/3 radius (1/3R), and ultradistal radius (UDR). T-scores compared subjects and controls with young-normal populations of the same race and sex, as provided by the manufacturer.

HR-pQCT of the distal radius and tibia

HR-pQCT (Xtreme CT, Scanco Medical AG, Brüttisellen, Switzerland) of the non-dominant distal radius and distal tibia (or non-fractured arm or leg in subjects with prior wrist or ankle fracture) was measured at CUMC as previously described.[11,13,16] The HR-pQCT measurement included 110 slices, corresponding to a 9.02-mm section along the axial direction, with a nominal isotropic voxel size of 82 μm. *After each scan, a reconstructed slide was examined immediately by the operator and grades the image quality from 1 to 5 (1= no motion artifact and 5=high wisping and major discontinuities. The subjects with severe movement artifact (>4) on the first scan were rescanned.* Analysis was performed according to the standard patient evaluation protocol, [35] and measurements were provided for total volumetric BMD (vBMD), trabecular bone volumetric BMD (Tb.BMD), cortical bone volumetric BMD (Ct.BMD), cortical thickness (Ct.Th), trabecular bone volume fraction (BV/TV), trabecular number (Tb.N), trabecular thickness (Tb.Th), and trabecular separation (Tb.Sp).

Cortical bone measurements

The cortical and trabecular regions were separated using a validated auto-segmentation custom method implemented in Image Processing language (IPL V5.07, Scanco Medical AG).[20] Cortical microarchitectural parameters were evaluated as follows.[21,22] Cortical porosity (Ct.Po, %) was calculated as the percentage of void space in the cortex. The number of pores was counted using component labeling, and the mean pore volume was calculated as the total volume of porosity divided by the pore number. The mean pore diameter (Ct.Po.Dm, mm) was calculated from the mean pore volume. Cortical thickness (Ct.Th, mm) was measured directly by removing the intracortical pores from the binary cortex image and using a distance transform. In addition, total bone area (Tot.Ar, mm^2), cortical bone area (Ct.Ar, mm^2), and trabecular bone area (Tb.Ar, mm^2) were calculated as the mean cross sectional area of total, cortical, and trabecular regions, respectively.

ITS-based morphological analyses

A complete volumetric decomposition technique was applied to segment the trabecular network into individual trabecular plates and rods.[23] Briefly, digital topological analysis (DTA)-based skeletonization was applied first to transform a trabecular bone image into a representation composed of surfaces and curves skeleton while preserving the topology (*i.e.*, connectivity, tunnels, and cavities), as well as plate and rod morphology of trabecular microarchitecture.[26,36] Then, digital topological classification was applied in which each skeletal voxel was uniquely classified as either a plate or a rod type.[25] Using an iterative reconstruction method, each voxel of the original image was classified as belonging to either

an individual plate or rod.[24] Based on the 3D evaluations of each individual trabecular plate or rod, plate and rod bone volume and number were evaluated by plate and rod bone volume fraction (pBV/TV and rBV/TV), as well as plate and rod number densities (pTb.N and rTb.N, 1/mm). Plate-to-rod ratio (P-R ratio), a parameter of plate versus rod characteristics of trabecular bone, was defined as plate bone volume divided by rod bone volume. The average size of plates and rods was quantified by plate and rod thickness (pTb.Th and rTb.Th, mm), plate surface area (pTb.S, mm^2), and rod length (rTb.ℓ, mm). Intactness of trabecular plate and rod network was characterized by plate–plate, plate–rod, and rod–rod junction density (P-P, P-R, and R-R Junc.D, $1/mm^3$), calculated as the total junctions between trabecular plates and rods normalized by the bulk volume. Orientation of trabecular bone network was characterized by axial bone volume fraction (aBV/TV). A trabecular plate was considered axially aligned if the angle between the normal vector of the plate and the axial direction was between 60° and 90°, and a rod was considered axially aligned if the angle between its normal vector and the axial direction was between 0° and 30°. aBV/TV was defined as the volume of axially aligned trabeculae divided by the bulk volume.[23]

HR-pQCT image-based μFEA

Both segmented binary HR-pQCT whole bone image and trabecular bone image of the distal radius and tibia were converted to whole bone and a trabecular bone μFE models.[16,37] Bone tissue was modeled as an isotropic, linear elastic material with a Young's modulus of 17 GPa and a Poisson's ratio of 0.3.[18,38] For each model of whole bone or trabecular bone segment, a uniaxial compression test using roller boundary condition was performed to calculate the reaction force under a displacement equal to 1% of bone segment height along the axial direction. FE solver (FAIM, v7.1; Numerics88, Calgary AB) on a desktop workstation (Linux CentOS 7.1, 2 × 6-core Intel Xenon, 64 GB RAM) was used to solve the models. Whole bone stiffness, defined as reaction force divided by the applied displacement, characterizes the mechanical competence of both cortical and trabecular compartments. Similarly, trabecular bone stiffness characterizes the mechanical competence of the trabecular bone compartment. The estimated failure loads of the whole bone and the trabecular bone compartment were computed based on a criterion developed by Pistoia et al.,[39] where fracture is assumed to occur when 2% of the bone tissue is strained beyond a strain threshold of 7000 microstrain.

Statistical methods

Analyses were conducted with NCSS software (NCSS Statistical Software, Kaysville, UT, USA). Descriptive data are presented as mean ± standard error of the mean (SEM). Differences between vertebral fracture and control subjects were assessed by Student's t test . Two-sided p-values <0.05 were considered to indicate statistical significance. Analysis of covariance (ANCOVA) was used to evaluate differences in HR-pQCT, ITS, cortical, and μFEA parameters at the radius or tibia after adjusting for aBMD T-score at the ultradistal radius or total hip, respectively and adjusting for vBMD at distal radius and tibia, respectively. ANOVA was also used to compare fracture versus non-fracture differences between the radius and tibia.

Logistic regression analysis was performed to estimate the relative risk of fracture associated with DXA, ITS, cortical, and FE parameters by using odds ratios (OR). Also, receiver operating characteristic (ROC) curve analysis was performed to determine the ability of the DXA, ITS, cortical, and FE parameters to discriminate the fracture subjects from controls. ITS parameters were used also as the independent variables in addition to aBMD a multiparametric model.

Results

Subject characteristics

Forty-five women with a history of postmenopausal vertebral fracture and 45 women with no fracture history were enrolled in this study. Subjects included 83% Caucasian, 8% African-American, and 9% from other backgrounds. Women with and without fractures did not differ on the basis of age, race or ethnicity, body mass index, or time since menopause (Table 1). Family history of osteoporosis was similar between groups. Alcohol and tobacco use, medication and supplement use, including use of calcium supplements, hormone replacement therapy, raloxifene, and thyroxine, did not differ between the fracture and control women. Use of vitamin D and bisphosphonates tended to be greater among women with vertebral fractures than in the control group, but the differences were not significant ($p=0.06$ and $p=0.13$, respectively)

Areal BMD

Mean *T*-score was in the osteopenic range, but above the WHO osteoporosis threshold (*T*-score ≤ -2.5), in vast majority of the subjects in both groups (Table 2). The prevalence of osteoporosis at any site was 49% among vertebral fracture subjects and 40% among controls. The prevalence of osteopenia at any site was 49% among vertebral fracture subjects and 44% among controls. Mean *T*-score tended to be lower at the LS in vertebral fracture subjects compared with controls, ($p=0.07$). At the FN, TH, and UDR, the mean *T*-score was 0.5~0.75 SD lower in women with vertebral fractures ($p<0.02$).

HR-pQCT

At both radius and tibia, women with vertebral fractures had significantly lower vBMD in the trabecular and cortical compartments compared with control subjects. Cortex was 17% and 21% thinner in the fracture subjects at radius and tibia, respectively. Fracture subjects had lower trabecular volume, fewer, thinner, and more widely spaced trabeculae compared with the control group. The differences in most of these parameters remained significant after adjustment for aBMD measurements (Table 3 and 4).

Trabecular microarchitecture by ITS analyses

Significant differences in trabecular plate and rod microarchitecture were detected between groups using ITS morphological analyses. At the distal radius, plate bone volume fraction and number (pBV/TV and pTb.N) were 21% and 9% lower in the vertebral fracture subjects, and rod bone volume fraction and number (rBV/TV and rTb.N) were 11% and 5% lower. The plate-rod ratio was 10% lower in the fracture subjects, though not significantly different from the control group ($p=0.20$). Junction density between plates and rods (P-P, P-R, and R-

R Junc. D) were 25%, 24%, and 14% lower in fracture subjects, indicating loss of trabecular connectivity compared with the controls. In contrast, the size of individual trabecular plates and rods did not differ significantly. Plate and rod thickness (pTb.Th and rTb.Th) were similar between groups. Plate surface area and rod length (pTb.S and rTb.ℓ) were 3% and 4% larger in fracture subjects ($p=0.04$ and <0.001, respectively). Axial bone volume fraction (aBV/TV), which reflects trabecular alignment along the axial direction, was 18% lower in fracture subjects than controls (Table 3, Figure 1). At the distal tibia, differences between the two groups were mainly observed in trabecular plate measurements: pBV/TV, pTb.N, P-R ratio, P-P Junc.D, P-R Junc.D, and aBV/TV were 20%, 7%, 18%, 19%, 15%, and 17% lower in vertebral fracture subjects. In contrast, rBV/TV, rTb.N, and R-R Junc.D did not differ between groups. Similar to findings at the radius, pTb.Th and rTb.Th did not differ between fracture and non-fracture subjects. After adjusting for aBMD, plate-related ITS measurements (pBV/TV, pTb.N, P-P Junc.D, P-R Junc.D, and aBV/TV) remained significantly lower in women with vertebral fractures at both distal radius and tibia (Table 4). Furthermore, pTb.N, rTb.ℓ, and P-R Junc.D at the radius remained significantly different between the fracture and control groups after adjusting for vBMD. Representative HR-pQCT scans analyzed by ITS are shown in Figure 2 for a vertebral fracture subject and a control subject, who were both 71 years old and had similar DXA T-scores.

Cortical microarchitecture

Women with vertebral fractures also had significant abnormalities in cortical microarchitecture. Fracture subjects had larger total bone area (6% at radius, 8% at tibia), larger trabecular bone area (12% at radius, 10% at tibia), and smaller cortical bone area (8% at radius, 11% at tibia) than women without fractures. Cortical thickness was 12% and 14% lower in fracture subjects at radius and tibia, respectively. Cortical porosity tended to be greater in fracture subjects ($p=0.11$, 0.07 at radius and tibia). Pore diameter did not differ between two groups. After adjusting for aBMD, only the total bone area and cortical thickness at the tibia remained significantly different between groups.

Stiffness by μFEA

Whole bone and trabecular bone stiffness were lower in women with vertebral fractures at both sites. At the radius, whole bone and trabecular bone stiffness were 18% and 22% lower, and the whole bone and trabecular bone estimated failure load were 13% and 16% lower in fracture subjects. At the tibia, whole bone and trabecular bone stiffness were 19% and 16% lower, and the whole bone and trabecular bone estimated failure load were 14% and 13% lower in fracture subjects. After adjustment for aBMD, whole bone stiffness and estimated failure load at the radius and tibia remained significantly lower, in fracture subjects, while trabecular bone stiffness and failure load no longer differed.

Logistic regression analyses

ORs assessed by logistic regression analyses and AUC assessed by ROC analyses suggested that HR-pQCT, ITS, and μFEA parameters were associated with vertebral fracture. Whole bone stiffness at the tibia had the highest OR of 3.44 (95% IC: 2.73~4.16) among all the independent variables, such that each SD decrease was associated with greater than a 3-fold risk of vertebral fracture; the AUC was 0.74. Estimated failure load at the tibia had an OR of

1.41 (95% IC: 1.04~1.78) and AUC of 0.71. Besides, whole bone stiffness and estimated failure load at the radius had ORs of 1.45 (95% IC: 1.23~1.66), and AUC of 0.71 and 0.69, respectively. Among HR-pQCT parameters, vBMD, Tb.BMD, and trabecular BV/TV showed strong predictive value with AUC from 0.73 to 0.76, comparable to some of the ITS parameters, including pBV/TV, aBV/TV, pTb.N, P-P Junc.D, and P-R Junc.D with ORs of 1.11~1.97 and AUC of 0.69~0.75. Furthermore, when combining aBMD at ultradistal radius or total hip with the ITS variables at radius or tibia, ROC analysis showed that the multiparametric models provided AUC of 0.81 at radius and 0.80 at tibia, respectively.

Discussion

In this study, we used morphological and mechanical analytic tools to identify abnormalities in trabecular plate and rod morphology and cortical bone structure in postmenopausal women with vertebral fractures. Using ITS analysis, we found that women with vertebral fractures had lower plate volume, lower plate trabecular number, reduced connectivity between plates and between plates and rods, and a less axially aligned trabecular network. They had thinner cortices and tended to have greater cortical porosity and lower stiffness. Differences in plate-related ITS measurements and whole bone stiffness remained significant after adjusting for aBMD by DXA.

ITS, cortical, and μFE analyses of HR-pQCT images have been previously validated in comparison with gold standard micro CT images.[12,40] Liu et al. reported that postmenopausal women with fragility fractures at the forearm, spine, ankle, and other sites had a prominent loss of trabecular plates, along with reduced stiffness at distal radius and tibia.[8] Our current study focused on women with vertebral fractures and increased the sample size, in order to provide further insights into the differences in trabecular and cortical microarchitecture, as well as bone stiffness between women with vertebral fractures and non-fracture controls. Our results demonstrated that women with vertebral fractures had abnormalities of both trabecular and cortical microarchitecture at both radius and tibia. By ITS analyses, we found the vertebral fracture subjects had major depletion of trabecular plates, loss of axially aligned trabeculae, and a trend toward a more rod-like trabecular network particularly at the tibia. Furthermore, the loss of trabecular plate bone volume fraction was mainly attributable to a decrease in plate trabecular number, while plate thickness did not differ. Cortical thinning in vertebral fracture subjects was the most prominent change we observed in cortical microarchitecture. Our observations in this study were consistent with findings from other studies of vertebral and nonvertebral fragility fractures.[9,11,41] Specifically, loss of trabecular plates and thin cortex were found to be two major microarchitectural characteristics in osteopenic women with fragility fractures.[33]

Abnormalities in trabecular plate microarchitecture were similar at the radius and tibia in the vertebral fracture subjects, but rod microarchitecture was altered only at the radius. This was consistent with several other studies that reported that tibia bone was relatively preserved compared to the radius, perhaps related to a protective effect of weight bearing.[8,9,11] When assessing different types of fractures, microarchitectural deterioration has often been more pronounced at the site that was more closely related anatomically to the fracture site. For example, changes in microarchitecture among women with wrist fractures were more

pronounced at the radius, and tibial trabecular microarchitectural abnormalities were more severe in women with ankle or hip fractures.[17,42] Recently, our lab measured trabecular microarchitecture and mechanical competence of the radius, tibia, and lumbar spine cadaver samples from the same donors and investigated the correlation between these sites. Our preliminary data showed that HR-pQCT of the radius was more strongly associated with stiffness at the spine, [43] which might help account for our finding that deterioration in trabecular microarchitecture was more pronounced at the radius in women with vertebral fractures.

Assessment of microarchitecture and mechanical competence increased our understanding of fragility fractures, and demonstrated that HR-pQCT-based ITS measurements had the ability to discriminate fractured postmenopausal women from non-fractured controls, and thus may be useful in predicting fracture risk. Vilayphiou et al. found that μFE-derived mechanical properties of the distal radius and tibia based on HR-pQCT images were associated with all types of fractures.[18] In particular, vertebral fracture was associated with trabecular microarchitecture more strongly than nonvertebral fracture. In this study, we found that several ITS parameters (pBV/TV, pTb.N, aBV/TV, P-P Junc.D, and P-R Junc.D) and whole bone stiffness had high ORs and AUC greater than 0.70, suggesting that they might have high predictive value in discriminating vertebral fracture subjects from non-fracture controls. Furthermore, differences in these plate-related ITS parameters and whole bone stiffness between fracture and control subjects were robust enough to remain significant after adjusting for aBMD *T*-score, which indicated that these microarchitectural and mechanical alterations in vertebral fracture subjects were independent of aBMD.

This study has several limitations. The cross-sectional study design cannot directly determine whether these methods can reliably predict incident vertebral fractures. Second, there are potential errors in evaluation of microarchitecture and μFE analysis due to the limited spatial resolution and signal-to-noise ratio of HR-pQCT. While validation studies have shown that ITS measurements and FE estimates based on HR-pQCT images are strongly correlated with those based on micro CT, there are errors associated with magnitudes of the parameters, especially for trabecular rods.[44]

In conclusion, our study demonstrated marked differences in plate and rod trabecular microarchitecture, cortical thickness, and stiffness at the radius and tibia between postmenopausal women with vertebral fractures and non-fractured controls. ITS analyses revealed a pattern of abnormalities consistent with those reported in other fracture types. Specifically, we found that preferential loss of trabecular plates, loss of axially aligned trabeculae, and loss of trabecular connectivity were the most prominent characteristics of women with vertebral fractures. Whole bone and trabecular bone stiffness, which reflects overall mechanical competence, were found to be markedly lower in women with vertebral fractures. Our results suggested that this pattern of abnormalities may contribute to bone fragility and increased susceptibility to vertebral fractures in postmenopausal women.

Acknowledgments

This work was supported by NIH R01 AR058004 (XEG and ES), NIH U01 AR055968 (ES), NIH K24 AR 052661 (ES), NIH K23 DK084337 (EMS). The author, Ji Wang, is supported by the Howard Hughes Medical Institute International Student Research Fellowship.

References

1. NIH Consensus Development Panel on Osteoporosis Prevention. Diagnosis, and Therapy, March 7–29, 2000: highlights of the conference. South Med J. 2001; 94(6):569–73. [PubMed: 11440324]
2. Johnell O, Kanis JA. An estimate of the worldwide prevalence and disability associated with osteoporotic fractures. Osteoporos Int. 2006; 17(12):1726–33. [PubMed: 16983459]
3. Melton LJ 3rd, Lane AW, Cooper C, Eastell R, O'Fallon WM, Riggs BL. Prevalence and incidence of vertebral deformities. Osteoporos Int. 1993; 3(3):113–9. [PubMed: 8481586]
4. Klotzbuecher CM, Ross PD, Landsman PB, Abbott TA 3rd, Berger M. Patients with prior fractures have an increased risk of future fractures: a summary of the literature and statistical synthesis. J Bone Miner Res. 2000; 15(4):721–39. [PubMed: 10780864]
5. Lindsay R, Silverman SL, Cooper C, Hanley DA, Barton I, Broy SB, Licata A, Benhamou L, Geusens P, Flowers K, Stracke H, Seeman E. Risk of new vertebral fracture in the year following a fracture. JAMA. 2001; 285(3):320–3. [PubMed: 11176842]
6. Roux C, Fechtenbaum J, Kolta S, Briot K, Girard M. Mild prevalent and incident vertebral fractures are risk factors for new fractures. Osteoporos Int. 2007; 18(12):1617–24. [PubMed: 17611706]
7. Melton LJ 3rd, Riggs BL, Keaveny TM, Achenbach SJ, Hoffmann PF, Camp JJ, Rouleau PA, Bouxsein ML, Amin S, Atkinson EJ, Robb RA, Khosla S. Structural determinants of vertebral fracture risk. J Bone Miner Res. 2007; 22(12):1885–92. [PubMed: 17680721]
8. Liu XS, Stein EM, Zhou B, Zhang CA, Nickolas TL, Cohen A, Thomas V, McMahon DJ, Cosman F, Nieves J, Shane E, Guo XE. Individual trabecula segmentation (ITS)-based morphological analyses and microfinite element analysis of HR-pQCT images discriminate postmenopausal fragility fractures independent of DXA measurements. J Bone Miner Res. 2012; 27(2):263–72. [PubMed: 22072446]
9. Sornay-Rendu E, Boutroy S, Munoz F, Delmas PD. Alterations of cortical and trabecular architecture are associated with fractures in postmenopausal women, partially independent of decreased BMD measured by DXA: the OFELY study. J Bone Miner Res. 2007; 22(3):425–33. [PubMed: 17181395]
10. Stein EM, Liu XS, Nickolas TL, Cohen A, McMahon DJ, Zhou B, Zhang C, Kamanda-Kosseh M, Cosman F, Nieves J, Guo XE, Shane E. Microarchitectural abnormalities are more severe in postmenopausal women with vertebral compared to nonvertebral fractures. J Clin Endocrinol Metab. 2012; 97(10):E1918–26. [PubMed: 22821893]
11. Stein EM, Liu XS, Nickolas TL, Cohen A, Thomas V, McMahon DJ, Zhang C, Yin PT, Cosman F, Nieves J, Guo XE, Shane E. Abnormal microarchitecture and reduced stiffness at the radius and tibia in postmenopausal women with fractures. J Bone Miner Res. 2010; 25(12):2572–81. [PubMed: 20564238]
12. Liu XS, Zhang XH, Sekhon KK, Adams MF, McMahon DJ, Bilezikian JP, Shane E, Guo XE. High-resolution peripheral quantitative computed tomography can assess microstructural and mechanical properties of human distal tibial bone. J Bone Miner Res. 2010; 25(4):746–56. [PubMed: 19775199]
13. Boutroy S, Bouxsein ML, Munoz F, Delmas PD. In vivo assessment of trabecular bone microarchitecture by high-resolution peripheral quantitative computed tomography. J Clin Endocrinol Metab. 2005; 90(12):6508–15. [PubMed: 16189253]
14. MacNeil JA, Boyd SK. Accuracy of high-resolution peripheral quantitative computed tomography for measurement of bone quality. Med Eng Phys. 2007; 29(10):1096–105. [PubMed: 17229586]
15. Melton LJ 3rd, Christen D, Riggs BL, Achenbach SJ, Muller R, van Lenthe GH, Amin S, Atkinson EJ, Khosla S. Assessing forearm fracture risk in postmenopausal women. Osteoporos Int. 2010; 21(7):1161–9. [PubMed: 19714390]

16. Boutroy S, Van Rietbergen B, Sornay-Rendu E, Munoz F, Bouxsein ML, Delmas PD. Finite element analysis based on in vivo HR-pQCT images of the distal radius is associated with wrist fracture in postmenopausal women. J Bone Miner Res. 2008; 23(3):392–9. [PubMed: 17997712]
17. Vico L, Zouch M, Amirouche A, Frere D, Laroche N, Koller B, Laib A, Thomas T, Alexandre C. High-resolution pQCT analysis at the distal radius and tibia discriminates patients with recent wrist and femoral neck fractures. J Bone Miner Res. 2008; 23(11):1741–50. [PubMed: 18665795]
18. Vilayphiou N, Boutroy S, Sornay-Rendu E, Van Rietbergen B, Munoz F, Delmas PD, Chapurlat R. Finite element analysis performed on radius and tibia HR-pQCT images and fragility fractures at all sites in postmenopausal women. Bone. 2010; 46(4):1030–7. [PubMed: 20044044]
19. Macneil JA, Boyd SK. Bone strength at the distal radius can be estimated from high-resolution peripheral quantitative computed tomography and the finite element method. Bone. 2008; 42(6): 1203–13. [PubMed: 18358799]
20. Buie HR, Campbell GM, Klinck RJ, MacNeil JA, Boyd SK. Automatic segmentation of cortical and trabecular compartments based on a dual threshold technique for in vivo micro-CT bone analysis. Bone. 2007; 41(4):505–15. [PubMed: 17693147]
21. Burghardt AJ, Kazakia GJ, Ramachandran S, Link TM, Majumdar S. Age- and gender-related differences in the geometric properties and biomechanical significance of intracortical porosity in the distal radius and tibia. J Bone Miner Res. 2010; 25(5):983–93. [PubMed: 19888900]
22. Nishiyama KK, Macdonald HM, Buie HR, Hanley DA, Boyd SK. Postmenopausal women with osteopenia have higher cortical porosity and thinner cortices at the distal radius and tibia than women with normal aBMD: an in vivo HR-pQCT study. J Bone Miner Res. 2010; 25(4):882–90. [PubMed: 19839766]
23. Liu XS, Sajda P, Saha PK, Wehrli FW, Bevill G, Keaveny TM, Guo XE. Complete volumetric decomposition of individual trabecular plates and rods and its morphological correlations with anisotropic elastic moduli in human trabecular bone. J Bone Miner Res. 2008; 23(2):223–35. [PubMed: 17907921]
24. Liu XS, Sajda P, Saha PK, Wehrli FW, Guo XE. Quantification of the roles of trabecular microarchitecture and trabecular type in determining the elastic modulus of human trabecular bone. J Bone Miner Res. 2006; 21(10):1608–17. [PubMed: 16995816]
25. Saha PK, Chaudhuri BB. 3D digital topology under binary transformation with applications. Computer Vision and Image Understanding. 1996; 63(3):418–29.
26. Saha PK, Chaudhuri BB, Dutta D, Majumder DD. A new shape preserving parallel thinning algorithm for 3D digital images. Pattern Recognition. 1997; 30(12):1939–55.
27. Liu XS, Bevill G, Keaveny TM, Sajda P, Guo XE. Micromechanical analyses of vertebral trabecular bone based on individual trabeculae segmentation of plates and rods. J Biomech. 2009; 42(3):249–56. [PubMed: 19101672]
28. Liu XS, Walker MD, McMahon DJ, Udesky J, Liu G, Bilezikian JP, Guo XE. Better skeletal microstructure confers greater mechanical advantages in Chinese-American women versus white women. J Bone Miner Res. 2011; 26(8):1783–92. [PubMed: 21351150]
29. Liu XS, Zhang XH, Guo XE. Contributions of trabecular rods of various orientations in determining the elastic properties of human vertebral trabecular bone. Bone. 2009; 45(2):158–63. [PubMed: 19379849]
30. Wang J, Kazakia GJ, Zhou B, Shi XT, Guo XE. Distinct Tissue Mineral Density in Plate and Rod-Like Trabeculae of Human Trabecular Bone. J Bone Miner Res. 2015
31. Wang J, Zhou B, Liu XS, Fields AJ, Sanyal A, Shi X, Adams M, Keaveny TM, Guo XE. Trabecular plates and rods determine elastic modulus and yield strength of human trabecular bone. Bone. 2015; 72:71–80. [PubMed: 25460571]
32. Wang J, Zhou B, Parkinson I, Thomas CDL, Clement JG, Fazzalari N, Guo XE. Trabecular Plate Loss and Deteriorating Elastic Modulus of Femoral Trabecular Bone in Intertrochanteric Hip Fractures. Bone Research. 2013; 1:346. [PubMed: 26273512]
33. Stein EM, Kepley A, Walker M, Nickolas TL, Nishiyama K, Zhou B, Liu XS, McMahon DJ, Zhang C, Boutroy S, Cosman F, Nieves J, Guo XE, Shane E. Skeletal structure in postmenopausal women with osteopenia and fractures is characterized by abnormal trabecular plates and cortical thinning. J Bone Miner Res. 2014; 29(5):1101–9. [PubMed: 24877245]

34. Genant HK, Wu CY, van Kuijk C, Nevitt MC. Vertebral fracture assessment using a semiquantitative technique. J Bone Miner Res. 1993; 8(9):1137–48. [PubMed: 8237484]

35. Laib A, Hauselmann HJ, Ruegsegger P. In vivo high resolution 3D-QCT of the human forearm. Technol Health Care. 1998; 6(5–6):329–37. [PubMed: 10100936]

36. Saha PK, Chaudhuri BB. DETECTION OF 3-D SIMPLE POINTS FOR TOPOLOGY PRESERVING TRANSFORMATIONS WITH APPLICATION TO THINNING. Ieee Transactions on Pattern Analysis and Machine Intelligence. 1994; 16(10):1028–32.

37. Liu XS, Zhang XH, Rajapakse CS, Wald MJ, Magland J, Sekhon KK, Adam MF, Sajda P, Wehrli FW, Guo XE. Accuracy of high-resolution in vivo micro magnetic resonance imaging for measurements of microstructural and mechanical properties of human distal tibial bone. J Bone Miner Res. 2010; 25(9):2039–50. [PubMed: 20499379]

38. Zysset PK, Guo XE, Hoffler CE, Moore KE, Goldstein SA. Mechanical properties of human trabecular bone lamellae quantified by nanoindentation. Technol Health Care. 1998; 6(5–6):429–32. [PubMed: 10100945]

39. Pistoia W, van Rietbergen B, Lochmüller EM, Lill CA, Eckstein F, Rüegsegger P. Estimation of distal radius failure load with micro-finite element analysis models based on three-dimensional peripheral quantitative computed tomography images. Bone. 2002; 30(6):842–8. [PubMed: 12052451]

40. Burghardt AJ, Buie HR, Laib A, Majumdar S, Boyd SK. Reproducibility of direct quantitative measures of cortical bone microarchitecture of the distal radius and tibia by HR-pQCT. Bone. 2010; 47(3):519–28. [PubMed: 20561906]

41. Sornay-Rendu E, Cabrera-Bravo JL, Boutroy S, Munoz F, Delmas PD. Severity of vertebral fractures is associated with alterations of cortical architecture in postmenopausal women. J Bone Miner Res. 2009; 24(4):737–43. [PubMed: 19113929]

42. Stein EM, Liu XS, Nickolas TL, Cohen A, Thomas V, McMahon DJ, Zhang C, Cosman F, Nieves J, Greisberg J, Guo XE, Shane E. Abnormal microarchitecture and stiffness in postmenopausal women with ankle fractures. J Clin Endocrinol Metab. 2011; 96(7):2041–8. [PubMed: 21508142]

43. Liu XS, Cohen A, Shane E, Yin PT, Stein EM, Rogers H, Kokolus SL, McMahon DJ, Lappe JM, Recker RR, Lang T, Guo XE. Bone density, geometry, microstructure, and stiffness: Relationships between peripheral and central skeletal sites assessed by DXA, HR-pQCT, and cQCT in premenopausal women. J Bone Miner Res. 2010; 25(10):2229–38. [PubMed: 20499344]

44. Liu XS, Shane E, McMahon DJ, Guo XE. Individual trabecula segmentation (ITS)-based morphological analysis of microscale images of human tibial trabecular bone at limited spatial resolution. J Bone Miner Res. 2011; 26(9):2184–93. [PubMed: 21557311]

Highlights

- Individual trabecula segmentation (ITS) was used to characterize trabecular plate and rod microarchitecture of postmenopausal women with vertebral fractures.
- Fractured patients had less trabecular plates, less axially aligned trabeculae and thinner cortical cortex compared to non-fractured controls.
- Bone stiffness and estimated failure load at the radius and tibia were reduced in women with vertebral fractures.

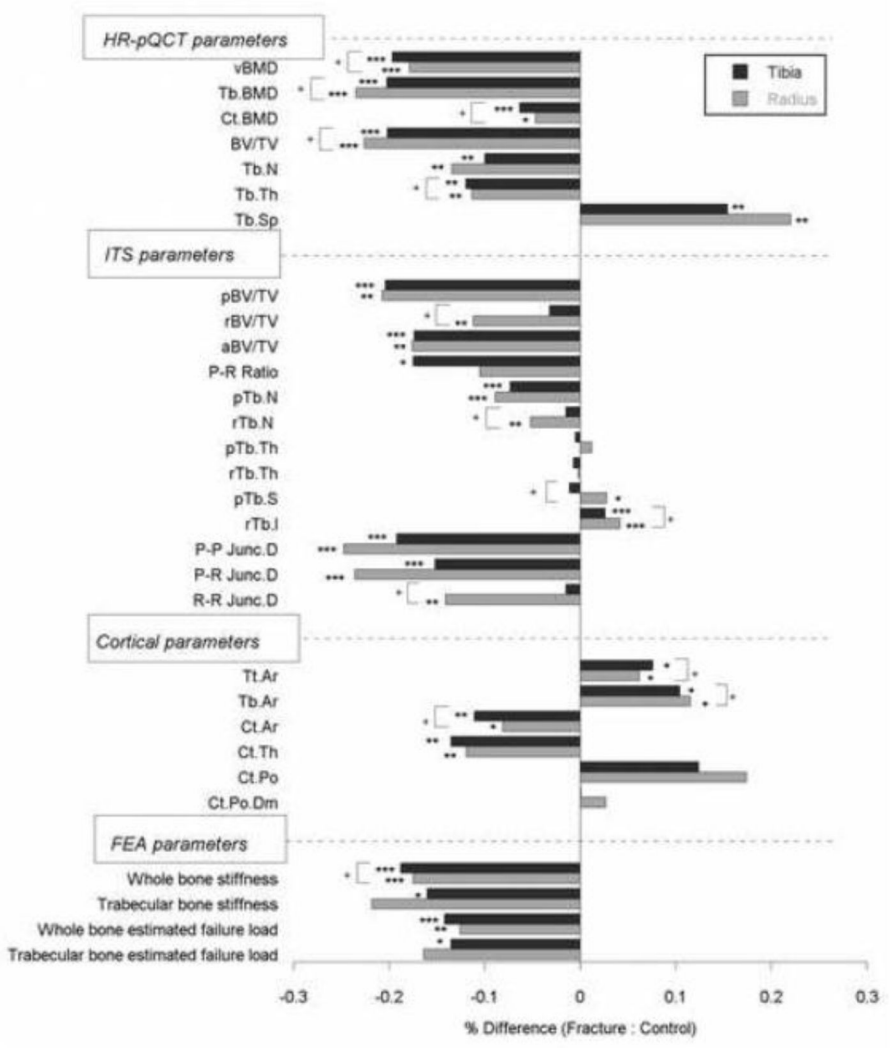

Figure 1.

Percent difference in HR-pQCT, ITS, cortical, and FEA parameters between women with vertebral fractures and controls. pBV/TV, plate bone volume fraction; rBV/TV, rod bone volume fraction; aBV/TV, axial bone volume fraction; P-R ratio, plate-rod volume ratio; pTb.N, trabecular plate number; rTb.N, trabecular rod number; pTb.Th, trabecular plate thickness; rTb.Th, trabecular rod thickness; pTb.S, trabecular plate surface area; rTb.l, trabecular rod length; P-P Junc. D, plate-plate junction density; P-R Junc.D, plate-rod junction density; R-R Junc.D, rod-rod junction density; Tt.Ar, total area; Tb.Ar, trabecular area; Ct.Ar, cortical area; Ct.Th, cortical thickness; Ct.Po, cortical porosity; Ct.Po.Dm, cortical pore diameter. (* $p<0.05$, ** $p<0.01$, *** $p<0.001$, fracture vs. control difference; + $p<0.05$, distal radius differs from distal tibia in fracture vs. control difference)

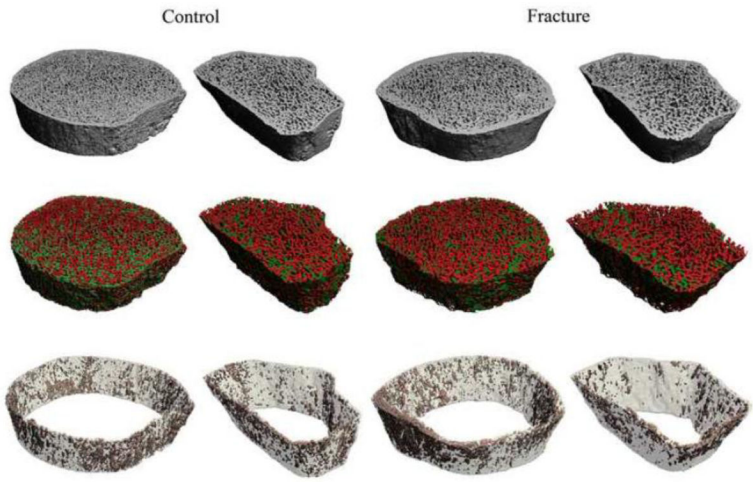

Figure 2.

Representative HR-pQCT scans at the tibia and radius of a vertebral fracture subject and a control subject who were both 71 years old and had similar DXA T-scores: (top) HR-pQCT image, (middle) trabecular compartment analyzed by ITS with plates in green and rods in red, (bottom) cortical compartment with bone tissue in light grey and pores in pink.

Table 1

Characteristics of the study population (Mean ± SEM)

	Vertebral fracture (n=45)	Control (n=45)	p
Age (years)	70 ± 1	70 ± 1	0.99
Race (%)			0.86
Caucasian	82	84	
African American	9	7	
Other	9	9	
Ethnicity (%)			0.79
Hispanic	20	18	
Non-Hispanic	80	82	
BMI (kg/m^2)	28 ± 1	27 ± 1	0.53
Years since menopause	22 ± 1	20 ± 1	0.46
Family history of osteoporosis by BMD (%)	40	33	0.78
Family history of fracture (%)	24	22	0.92
Tobacco use (%)			0.24
Never	47	33	
Former	38	47	
Current	7	2	
Alcohol use (beverages per day)	0.5 ± 0.1	0.8 ± 0.2	0.90
Calcium supplements, total daily dose (mg)	635 ± 100	593 ± 90	0.75
Vitamin D supplements, total daily dose (IU)	1233 ± 279	804 ± 228	0.06
Hormone replacement therapy (%)			
Past	38	40	0.46
Current	4	4	0.94
Bisphosphonates[a] (%)			
Past	13	4	0.13
Current	13	4	0.13
Raloxifene (%)	7	4	0.76
Thyroxine (%)	18	24	0.27

[a]Prior bisphosphonate use limited to <1 year

Table 2

DXA T-score in vertebral fracture subjects and controls

DXA *T*-score	Vertebral Fracture (Mean ± SEM)	Control (Mean ± SEM)	*p*-Value	OR (95% CI)	AUC
Lumbar spine	−1.81 ± 0.23	−1.26 ± 0.19	0.07	1.03 (0.94, 1.12)	0.60
Total hip	−1.55 ± 0.15	−0.98 ± 0.16	0.02	1.13 (0.96, 1.30)	0.66
Femoral neck	−2.05 ± 0.11	−1.53 ± 0.14	0.01	1.19 (0.98, 1.40)	0.66
1/3 radius	−1.65 ± 0.21	−1.39 ± 0.19	0.38	1.00 (0.96, 1.04)	0.54
Ultradistal radius	−1.75 ± 0.16	−1.00 ± 0.21	0.005	1.21 (1.02, 1.40)	0.67

Table 3

HR-pQCT, ITS, cortical, and mechanical parameters at distal radius in vertebral fracture subjects and controls

Variables	Vertebral Fracture (Mean ± SEM)	Control (Mean ± SEM)	*p*-Value	OR (95% CI)	AUC
HR-pQCT					
			<0.001[b]		
vBMD (mg HA/cm^3)	250 ± 8	304 ± 10		1.35 (1.09, 1.61)	0.73
Tb.BMD (mg HA/cm^3)	107 ± 5	140 ± 6	<0.001[c]	1.45 (1.13, 1.77)	0.74
Ct.BMD (mg HA/cm^3)	812 ± 12	852 ± 10	<0.001	1.11 (0.95, 1.68)	0.63
BV/TV	0.090 ± 0.005	0.116 ± 0.005	<0.001[b]	1.39 (1.10, 1.68)	0.73
Tb.N (1/mm)	1.587 ± 0.055	1.832 ± 0.049	0.001[a]	1.26 (1.02, 1.49)	0.69
Tb.Th (mm)	0.056 ± 0.002	0.063 ± 0.001	0.002[a]	1.18 (0.99, 1.36)	0.71
Tb.Sp (mm)	0.613 ± 0.029	0.502 ± 0.017	0.001[a]	1.81 (0.89, 2.73)	0.69
ITS					
pBV/TV	0.082 ± 0.005	0.103 ± 0.005	0.002[a]	1.11 (0.98, 1.25)	0.69
rBV/TV	0.137 ± 0.005	0.154 ± 0.004	0.007	1.13 (0.97, 1.29)	0.66
aBV/TV	0.089 ± 0.004	0.108 ± 0.004	0.002[a]	1.17 (1.00, 1.34)	0.70
P-R ratio	0.611 ± 0.040	0.684 ± 0.038	0.12	0.96 (0.91, 1.01)	0.62
pTb.N (1/mm)	1.224 ± 0.022	1.344 ± 0.021	<0.001[b,*]	1.34 (1.09, 1.58)	0.73
rTb.N (1/mm)	1.765 ± 0.023	1.862 ± 0.021	0.003	1.21 (1.00, 1.41)	0.69
pTb.Th (mm)	0.222 ± 0.002	0.220 ± 0.001	0.14	0.99 (0.91, 1.06)	0.56
rTb.Th (mm)	0.208 ± 0.001	0.209 ± 0.001	0.46	0.94 (0.92, 0.95)	0.55
pTb.S (mm^2)	0.191 ± 0.002	0.186 ± 0.001	0.04	1.07 (0.93, 1.21)	0.63
rTb.ℓ (mm)	0.660 ± 0.005	0.633 ± 0.004	<0.001[b,*]	1.48 (1.11, 1.85)	0.74
P-P Junc.D (1/mm^3)	1.344 ± 0.074	1.786 ± 0.083	<0.001[b]	1.29 (1.08, 1.50)	0.74
P-R Junc.D (1/mm^3)	2.830 ± 0.139	3.705 ± 0.157	<0.001[b,*]	1.35 (1.11, 1.59)	0.74
R-R Junc.D (1/mm^3)	2.595 ± 0.111	3.021 ± 0.108	0.007	1.12 (0.97, 1.27)	0.67
Cortical					
Tt.Ar (mm^2)	244 ± 6	230 ± 5	0.05	1.04 (0.92, 1.16)	0.62

Variables	Vertebral Fracture (Mean ± SEM)	Control (Mean ± SEM)	*p*-Value	OR (95% CI)	AUC
Tb.Ar (mm^2)	203 ± 6	182 ± 5	0.02	1.21 (0.97, 1.44)	0.65
Ct. Ar (mm^2)	47 ± 1	51 ± 1	0.02	1.08 (0.97, 1.20)	0.63
Ct.Th (mm)	0.783 ± 0.024	0.889 ± 0.026	0.003	1.18 (1.00, 1.36)	0.70
Ct.Po	0.055 ± 0.004	0.047 ± 0.003	0.11	1.02 (0.94, 1.11)	0.60
Ct.Po.Dm (mm)	0.154 ± 0.003	0.150 ± 0.003	0.16	0.99 (0.93, 1.04)	0.58
FEA					
Whole bone stiffness (N/mm)	68,158 ± 2,495	82,642 ± 2,883	<0.001[b]	1.45 (1.23, 1.66)	0.71
Trabecular bone stiffness (N/mm)	14,551 ±1,586	18,601 ± 1,402	0.06	0.99 (0.92, 1.07)	0.65
Whole bone estimated failure load (N)	4,397 ± 124	5031 ± 143	0.001[a]	1.15 (0.98, 1.32)	0.69
Trabecular bone estimated failure load (N)	942 ± 81	1,126 ± 68	0.08	1.00 (0.93, 1.07)	0.61

[a] p<0.05,

[b] p<0.01,

[c] p<0.001, group difference remains significant after adjusting for aBMD at ultradistal radius;

[*] p<0.05, group difference remains significant after adjusting for vBMD at distal radius.

Bone. Author manuscript; available in PMC 2017 July 01.

Table 4

HR-pQCT, ITS, cortical, and mechanical parameters at distal tibia in vertebral fracture subjects and controls

Variables	Vertebral Fracture (Mean ± SEM)	Control (Mean ± SEM)	*p*-Value	OR (95% CI)	AUC
HR-pQCT					
vBMD (mg HA/cm^3)	201 ± 7	251 ± 6	<0.001[c]	1.48 (1.13, 1.83)	0.76
Tb.BMD (mg HA/cm^3)	122 ± 5	153 ± 5	<0.001[c]	1.63 (1.23, 2.03)	0.74
Ct.BMD (mg HA/cm^3)	742 ± 11	792 ± 9	<0.001[a]	1.35 (1.09, 1.61)	0.68
BV/TV	0.102 ± 0.004	0.127 ± 0.004	<0.001[c]	1.77 (1.31, 2.34)	0.74
Tb.N (1/mm)	1.551 ± 0.046	1.723 ± 0.042	0.007	1.18 (1.02, 1.34)	0.69
Tb.Th (mm)	0.066 ± 0.002	0.074 ± 0.002	0.001[c]	1.28 (1.07, 1.49)	0.68
Tb.Sp (mm)	0.604 ± 0.021	0.523 ± 0.016	0.003	1.41 (1.05, 1.78)	0.69
ITS					
pBV/TV	0.118 ± 0.006	0.148 ± 0.006	<0.001[b]	1.37 (1.12, 1.62)	0.73
rBV/TV	0.122 ± 0.005	0.127 ± 0.004	0.19	0.99 (0.96, 1.02)	0.55
aBV/TV	0.116 ± 0.004	0.140 ± 0.004	<0.001[b]	1.45 (1.15, 1.74)	0.73
P-R ratio	1.041 ± 0.073	1.261 ± 0.084	0.02	1.05 (0.97, 1.13)	0.61
pTb.N(1/mm)	1.356 ± 0.018	1.463 ± 0.016	<0.001[c]	1.97 (1.26, 2.67)	0.74
rTb.N(1/mm)	1.702 ± 0.023	1.728 ± 0.021	0.41	0.99 (0.96, 1.03)	0.56
pTb.Th(mm)	0.231 ± 0.001	0.232 ± 0.001	0.56	0.99 (0.96, 1.01)	0.56
rTb.Th(mm)	0.212 ± 0.001	0.213 ± 0.001	0.33	1.00 (0.95, 1.04)	0.52
pTb.S (mm^2)	0.198 ± 0.002	0.200 ± 0.002	0.63	0.99 (0.96, 1.02)	0.52
rTb.l (mm)	0.635 ± 0.004	0.619 ± 0.003	<0.001[b]	1.41 (1.10, 1.71)	0.70
P-P Junc.D (1/mm^3)	1.742 ± 0.061	2.156 ± 0.065	<0.001[c]	1.74 (1.28, 2.20)	0.75
P-R Junc.D (1/mm^3)	3.193 ± 0.101	3.766 ± 0.112	<0.001[b]	1.36 (1.12, 1.59)	0.71
R-R Junc.D (1/mm^3)	2.238 ± 0.117	2.272 ± 0.097	0.82	0.98 (0.97, 0.99)	0.56
Cortical					
Tt.Ar (mm^2)	719 ± 19	668 ± 13	0.03[a]	1.13 (0.96, 1.29)	0.63
Tb.Ar (mm^2)	636 ± 19	577 ± 14	0.01	1.20 (0.98, 1.42)	0.65

Variables	Vertebral Fracture (Mean ± SEM)	Control (Mean ± SEM)	*p*-Value	OR (95% CI)	AUC
Ct. Ar (mm^2)	87 ± 2	98 ± 3	0.006	1.18 (1.02, 1.34)	0.63
Ct.Th (mm)	0.912 ± 0.029	1.054 ± 0.032	0.001[a]	1.28 (1.07, 1.50)	0.67
Ct.Po	0.113 ± 0.005	0.101 ± 0.005	0.07	1.06 (0.97, 1.15)	0.60
Ct.Po.Dm (mm)	0.180 ± 0.003	0.180 ± 0.002	0.96	0.98 (0.98, 0.98)	0.52
FEA					
Whole bone stiffness (N/mm)	199,435 ± 6,533	245,471 ± 7,649	<0.001[c]	3.44 (2.73, 4.16)	0.74
Trabecular bone stiffness (N/mm)	94,106 ± 5,565	112,027 ± 6,093	0.03	1.46 (1.37, 1.56)	0.61
Whole bone estimated failure load (N)	11,390 ± 292	13,276 ± 368	<0.001[b]	1.41 (1.04, 1.78)	0.71
Trabecular bone estimated failure load (N)	5,056 ± 267	5,847 ± 274	0.04	1.11 (1.08, 1.20)	0.63

[a] $p<0.05$,

[b] $p<0.01$,

[c] $p<0.001$, group difference remains significant after adjustment for aBMD at total hip.